



# Broadband antireflection coatings for visible and infrared ranges

Frédéric Lemarquis<sup>1</sup> · Thomas Begou<sup>1</sup> · Antonin Moreau<sup>1</sup> · Julien Lumeau<sup>1</sup>

Received: 11 March 2019 / Revised: 21 June 2019 / Accepted: 3 July 2019 / Published online: 15 July 2019  
© CEAS 2019

## Abstract

Antireflection coatings are critical elements for space applications as they will influence the overall performances of optical systems. They are among the most classical elements that are produced with optical coatings but remain a challenge when high performances are required. In this paper, we present some recent results based on thin film technology for the production of antireflection coatings dedicated to visible, near-IR and mid-IR spectral ranges. We first present a theoretical and experimental study of broadband antireflection coatings for (400–1100)-nm spectral range. We then show antireflection coatings covering the (1.5–15)- $\mu\text{m}$  range. Experimental demonstrations and limitations are presented.

**Keywords** Optical coatings · Antireflection coatings · Thin film design · Physical vapor deposition

## 1 Introduction

Antireflection coatings are among the most common and widely spread optical coatings that are used in every optical system to decrease losses and prevent shadow images. For space applications, they are critical elements which specifications will highly influence the overall optical system performances. Despite the very wide range of developments that have been carried out over the past 30 years [1–5], the production of broadband antireflection coatings for visible and infrared ranges remains a challenge and the requirements issued from the space community are frequently at the limit if not beyond theoretical and manufacturing capabilities. One goal of this paper is to give an overview of what can be achieved in terms of performance in both the visible, NIR and mid-IR spectral ranges. Actually, while optical coatings can, in theory, provide perfect antireflection function at a single wavelength, the final performances will then be highly affected by the width of the spectral range of interest [2, 6]. There are some various rules of thumb when it comes to the design of antireflection coatings.

- The average residual reflection that can be achieved with multilayer structures depends on the required spectral

range, the broader this range, the higher the residual reflection.

- The performances that can be achieved depend on the refractive index of the materials used in the design. The best results are obtained using the lowest and highest possible indices. For this reason, considering oxide materials, the combination of  $\text{SiO}_2$  and  $\text{Nb}_2\text{O}_5$  (or eventually  $\text{TiO}_2$ ) ( $n \approx 1.47$  and  $2.35$ ) appears, to date, as the best solution for the visible and near-IR ranges, e.g., 400–1100 nm. Fluoride materials, with a lower refractive index, can help achieve a better optical result, but their use raises some technological issues.
- If broader spectral range is needed and especially going down to 300 nm, due to the absorption of  $\text{Nb}_2\text{O}_5$  in the UV range,  $\text{Nb}_2\text{O}_5$  should be replaced with  $\text{HfO}_2$  ( $n \approx 2.05$ ) to cover, for example, the (300–1100)-nm spectral range. The refractive index being lower, and the spectral range extended, the residual reflection will then be higher. When it comes to extending the spectral range to longer wavelength, due to absorption of oxide materials above 2.5  $\mu\text{m}$ , it is then required to use sulfide and/or fluoride materials. For this purpose, the use of  $\text{ZnS}$  and  $\text{YF}_3$  appears as one of the most appropriate couple of materials available today. However, absorption of  $\text{YF}_3$  in some spectral ranges will affect the coating performances within these ranges.
- The performances of antireflection coatings are very sensitive to thickness variations of the layers. As a consequence, increasing the number of layers of a coating

✉ Julien Lumeau  
julien.lumeau@fresnel.fr

<sup>1</sup> Aix Marseille Univ, CNRS, Centrale Marseille, Institut Fresnel, 13013 Marseille, France

stack to theoretically improve its spectral performances might finally result, when considering manufacturing thickness errors, in poorer performances than a simpler design. In conclusion, the production of high-performance antireflection coatings requires an accurate control of the thickness of each of the layers of the stack.

In this paper, we demonstrate the performances that can be achieved in the design and the fabrication of high-performance broadband antireflection coatings with today's technology.

## 2 Results and discussion

Four types of antireflection coatings have been considered in this study:

- An antireflection coating for silica substrates optimized for normal incidence and covering the (400–1200)-nm spectral range.
- An antireflection coating for silica substrates optimized for 45° oblique incidence and covering the (400–900)-nm spectral range.
- An antireflection coating for silica substrates optimized for a beam aperture up to  $\pm 50^\circ$  incidence and covering the (400–800)-nm spectral range.
- An antireflection coating for ZnSe substrates optimized for normal incidence and covering the (1.5–15)- $\mu\text{m}$  spectral range.

The two major differences between these antireflection coatings for the visible/NIR and mid-IR spectral ranges are the following:

- Low-index substrates such as silica are frequently used in the visible/NIR range and the refractive index of the high-index coating material is then much higher than that of the substrate. On the contrary, high-index substrates such as ZnSe or Ge are frequently used in the mid-IR range, so that both layer materials indices are in between the substrate and air index values. One consequence is that the coating designs are completely different, with a limited maximum spectral range in case of low-index substrate, and much wider capabilities in case of high-index substrates.
- Oxide materials are fully transparent in the visible/NIR spectral range and are fully compatible with ion-assisted or sputtering deposition techniques, resulting in excellent mechanical and environmental behavior of the coatings, which is of great importance for space applications. Unfortunately, these materials are no more transparent in the mid-IR range for which classical layer materials are

Ge, ZnS, and fluorides. Since these materials are far less compliant with high-energy deposition techniques, they are still most often deposited with classical evaporation, leading to poorer mechanical and environmental characteristics.

Below, we provide a description of the design, the fabrication and the limitations of each type of antireflection coatings.

### 2.1 Visible/near-IR antireflection coating for normal incidence

The first coating that has been studied is an antireflection coating optimized for the spectral band between 400 and 1200 nm, operating at normal incidence. For this study, we considered  $\text{Nb}_2\text{O}_5$  and  $\text{SiO}_2$  as the high and low-refractive index materials for layers, and fused silica as the substrate. We designed different structures to produce this function and have plotted in Fig. 1 the spectral performances in reflection of each of these designs. These designs are composed of 10, 20, 28 and 34 layers and correspond, respectively, to stacks with total thickness of  $\sim 400$ , 800, 1200 and 1600 nm. All stacks do not show any periodicity and have layers with thicknesses ranging from 5 to  $\sim 150$  nm. These designs have been obtained using a numerical approach, namely the needle technique [7].

At first, the minimum number of layers required to achieve such performances is equal to  $\sim 10$ . With such a stack, the average reflection coefficient is equal to  $\sim 1\%$ . Increasing the number of layers of the stack allows slightly decreasing the residual reflection to a level of  $\sim 0.8\%$ . Such a residual reflection coefficient is the lowest theoretical value that can be achieved with a multilayer structure based on standard oxide materials (see first and second rules of thumb) and further increasing the spectral range of interest would further increase this residual reflection. In this paper, we considered a formula with 20 alternated high- and low-refractive index layers (Table 1).

It can be seen that the formula has no periodicity as well as large variations in thickness ( $30\times$  change). There are also very thin layers: the first layer has a thickness of 5 nm and 8 layers have thicknesses lower than 20 nm. As mentioned previously, such a structure is very sensitive to errors on layer thicknesses. Its fabrication requires a very good control of the thickness of each of the layers.

This coating has been manufactured within the *Espace Photonique* platform of *Institut Fresnel* [8], using a Bühler HELIOS machine in which low- and high-refractive index materials were both deposited through Plasma-Assisted Reactive Magnetron Sputtering (PARMS) [9]. The main chamber is subdivided into different treatment zones, two dedicated to dielectric materials (MF magnetron

**Fig. 1** Spectral reflectance of visible/near-IR Nb<sub>2</sub>O<sub>5</sub>/SiO<sub>2</sub> antireflection coatings for normal incidence made with an increasing number of layers

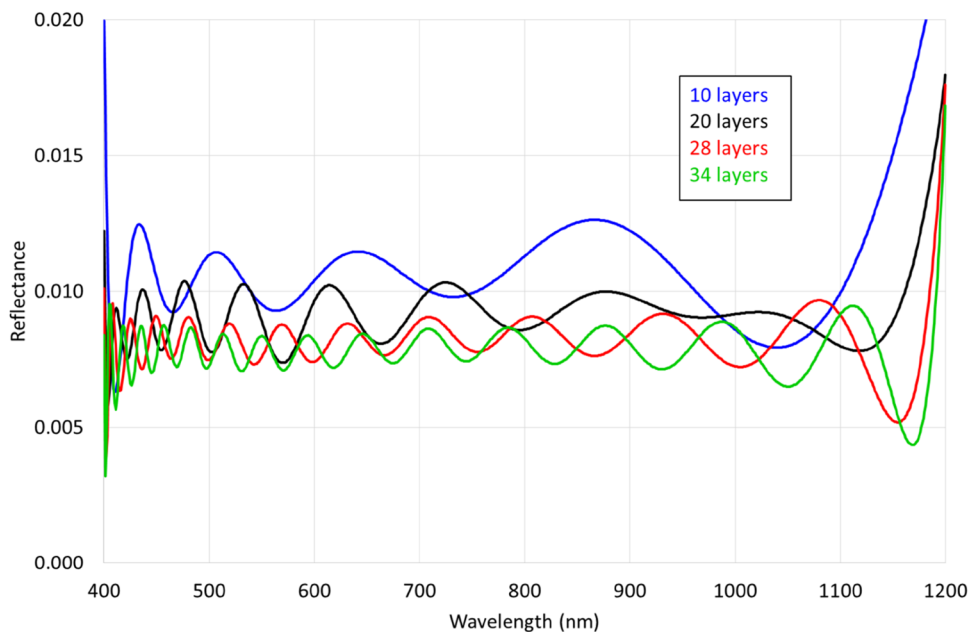


**Table 1** Layer thicknesses of visible/near-IR antireflection coating for zero incidence

Layer #	1	2	3	4	5	6	7	8	9	10
Material	Nb <sub>2</sub> O <sub>5</sub>	SiO <sub>2</sub>	Nb <sub>2</sub> O <sub>5</sub>	SiO <sub>2</sub>	Nb <sub>2</sub> O <sub>5</sub>	SiO <sub>2</sub>	Nb <sub>2</sub> O <sub>5</sub>	SiO <sub>2</sub>	Nb <sub>2</sub> O <sub>5</sub>	SiO <sub>2</sub>
Thickness (nm)	5	74.2	18	43.6	38.2	15.4	86.2	13.9	38.8	47.5
Layer #	11	12	13	14	15	16	17	18	19	20
Material	Nb <sub>2</sub> O <sub>5</sub>	SiO <sub>2</sub>	Nb <sub>2</sub> O <sub>5</sub>	SiO <sub>2</sub>	Nb <sub>2</sub> O <sub>5</sub>	SiO <sub>2</sub>	Nb <sub>2</sub> O <sub>5</sub>	SiO <sub>2</sub>	Nb <sub>2</sub> O <sub>5</sub>	SiO <sub>2</sub>
Thickness (nm)	13.9	143.8	9.1	56.7	32.7	17.8	86	17.9	28.7	108.1

sputtering), and one to oxygen plasma assistance (PBS). The substrates are set on a 12-position rotating sample holder (rotation at 240 rpm). According to the deposited material, either low or high index, the corresponding MF magnetron sputtering cathode is switched on. The oxygen plasma assistance is used for densification of the coating and also to respect the stoichiometry of the layers. Typical deposition rates of low- and high-index materials are, respectively, around 0.40–0.45 nm s<sup>-1</sup> and 0.50–0.60 nm s<sup>-1</sup>. The control of the thickness of each of the layers was carried out using a Bühler OMS 5100 optical monitoring system interfaced with the HELIOS machine [10]. The HELIOS machine being equipped with a load-lock system, several monitoring test glasses can be used during the fabrication. We developed an all-optical monitoring strategy using custom software [11, 12], based on the use of two different test glasses:

- layers 1–8: optical monitoring at 410 nm on test glass 1;
- layers 9–20: optical monitoring at 470 nm on test glass 2.

The use of an all-optical monitoring strategy was shown to provide minimum errors on the thickness of each layer even for the thinnest layers. We fabricated a prototype on the HELIOS machine using the above-mentioned strategy (Run 1) and measured the spectrum of the filter using a Perkin Elmer Lambda 1050 (Fig. 2). It can be seen that using this method, we have been able to fabricate a visible/near-IR antireflection coating for normal incidence with very low manufacturing errors, thus making it possible to minimize the Fresnel reflection of a fused silica substrate with performances close to those predicted by the theory.

To further characterize the performances of the antireflection coatings and also test the repeatability of the manufacturing process, a new deposition run was performed (Run 2). Two types of samples were generated: a new single-side antireflection-coated sample and a dual-side antireflection-coated sample (Runs 1 + 2). The performances of the new single-side antireflection coating were characterized and compared with those of the first coating run (Fig. 3).

The stability of the deposition rates of the HELIOS machine combined with an efficient optical monitoring

**Fig. 2** Comparison of the theoretical and measured spectral transmission of a single-side visible/near-IR antireflection coating for normal incidence monitored with two test glasses (Run 1) (uncoated rear side)

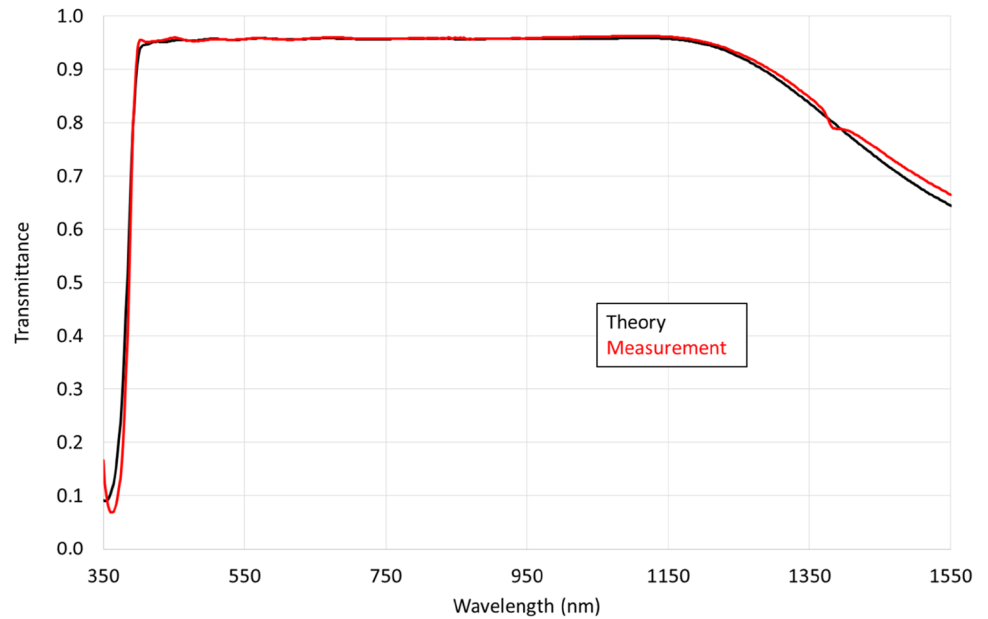
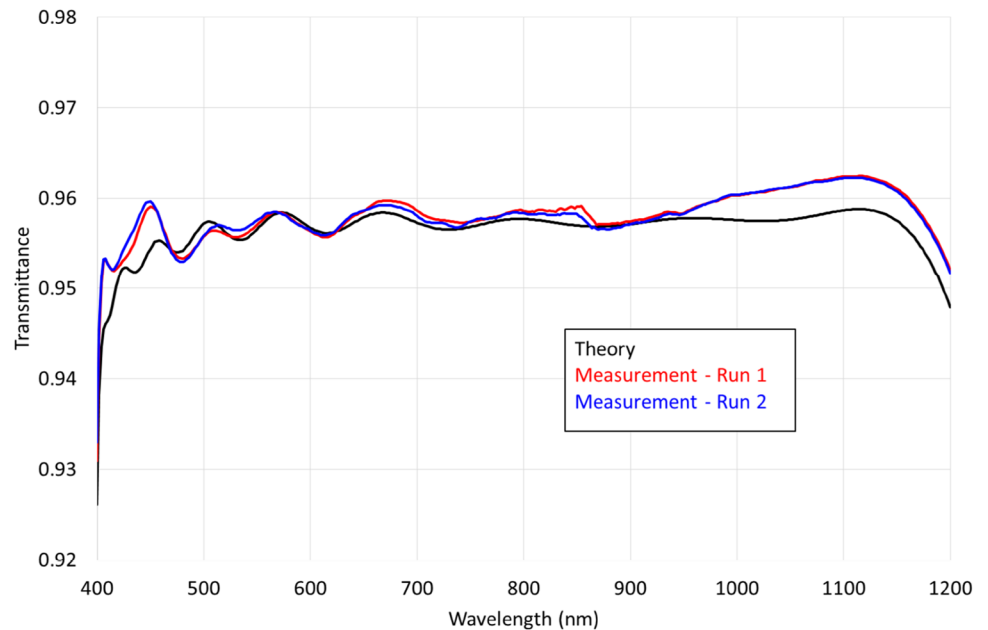


**Fig. 3** Spectral transmission of visible/near-IR antireflection coating for normal incidence monitored with two test glasses (Runs 1 and 2)



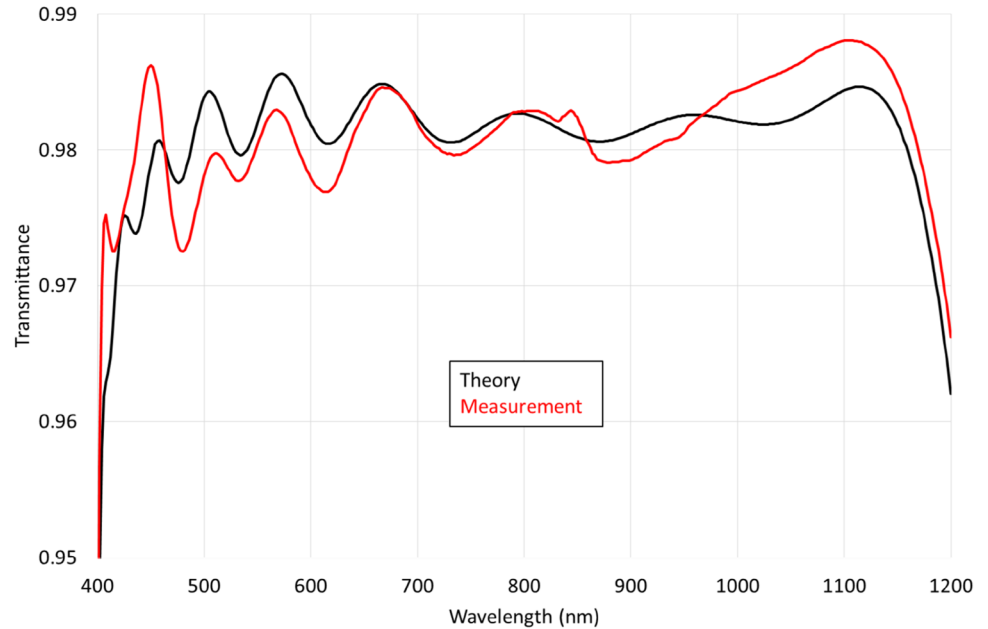
strategy makes it possible to guarantee optimal repeatability from one deposition to another. Finally, we measured the spectral response of the dual-side component (Fig. 4). In conclusion, the developed multilayer structures can guarantee an average transmittance of the order of 98.2% with fluctuations not exceeding 1% over the spectral range 400–1100 nm. It is worth noting that an error analysis based on 3% average standard deviation random errors (representative of crystal quartz monitoring) showed that such experimental/theoretical agreement could not be achieved. In other words, this result demonstrates that the average error on the thickness of each layer is very low. However, as the errors on

the thickness of each layer are correlated due to the optical monitoring technique, it is hard to precisely quantify those errors.

## 2.2 Visible/near-IR antireflection coating for oblique incidence

The second antireflection structure that has been studied was optimized for the spectral band between 400 and 900 nm and for the angle of incidence of 45°. Actually, the increase of the angle of incidence produces a spectral shift toward blue and a separation of spectral responses in S and

**Fig. 4** Spectral transmission of a dual-side visible/near-IR antireflection-coated window for normal incidence



P polarization. As a general result, the S reflectance is higher than the P one.

We again considered Nb<sub>2</sub>O<sub>5</sub> and SiO<sub>2</sub> as the high- and low-refractive index materials for layers, and fused silica as the substrate. The designed structure is given in Table 2. It is composed of 34 layers with a wide range of thicknesses.

We have plotted in Fig. 5 the spectral dependence of the reflection at 45° of the designed antireflection structure of Table 2. The design has been optimized for the S polarization only, leading to a reflectance almost constant around 1% for this polarization. As mentioned before, the reflectance for P polarization is most often lower, except close to the boundary of the considered spectral range. The performances obtained for non-polarized light are similar to the

performances that can be achieved when optimizing simultaneously for S and P polarizations.

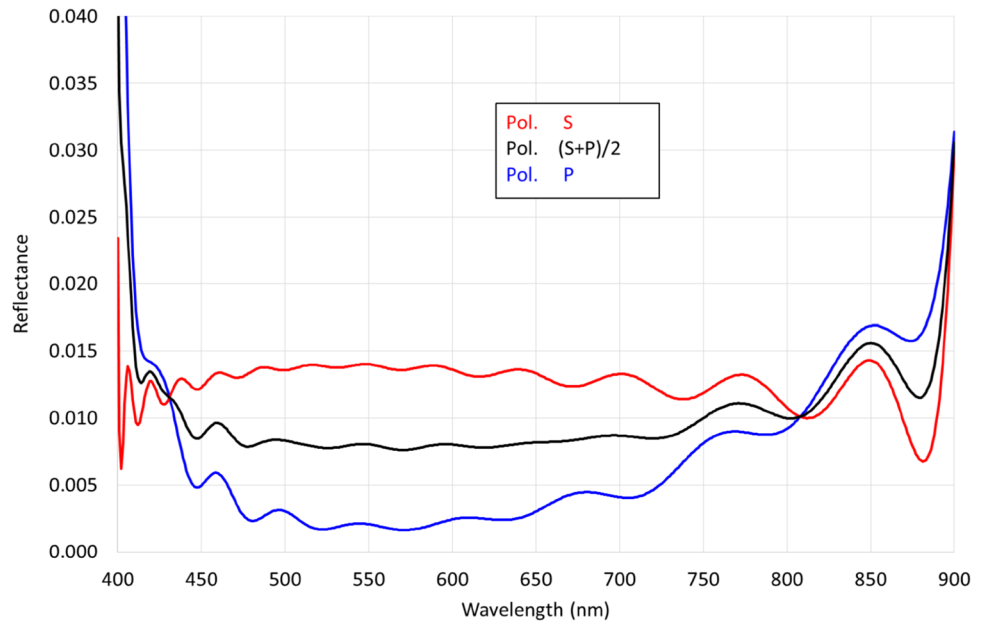
We then experimentally demonstrated this antireflection coating. To minimize the fabrication errors, we opted for an all-optical monitoring strategy based on the use of three consecutive test glasses. A first test glass is used to monitor the first 12 layers, a second glass for the next 12 and a third glass for the last 10. We then determined the following monitoring strategy:

- layers 1–12: optical monitoring at 430 nm on test glass 1;
- layers 13–24: optical monitoring at 505 nm on test glass 2;

**Table 2** Layer thicknesses of visible/near-IR antireflection coating for oblique incidence (45°)

Layer #	1	2	3	4	5	6	7	8	9	10
Material	Nb <sub>2</sub> O <sub>5</sub>	SiO <sub>2</sub>	Nb <sub>2</sub> O <sub>5</sub>	SiO <sub>2</sub>	Nb <sub>2</sub> O <sub>5</sub>	SiO <sub>2</sub>	Nb <sub>2</sub> O <sub>5</sub>	SiO <sub>2</sub>	Nb <sub>2</sub> O <sub>5</sub>	SiO <sub>2</sub>
Thickness (nm)	5.3	70.1	22.5	30.1	79.5	11.4	38.3	59.3	6.8	146
Layer #	11	12	13	14	15	16	17	18	19	20
Material	Nb <sub>2</sub> O <sub>5</sub>	SiO <sub>2</sub>	Nb <sub>2</sub> O <sub>5</sub>	SiO <sub>2</sub>	Nb <sub>2</sub> O <sub>5</sub>	SiO <sub>2</sub>	Nb <sub>2</sub> O <sub>5</sub>	SiO <sub>2</sub>	Nb <sub>2</sub> O <sub>5</sub>	SiO <sub>2</sub>
Thickness (nm)	25.2	24.1	76.2	35.4	18.5	131.3	17	37.1	78.9	23.5
Layer #	21	22	23	24	25	26	27	28	29	30
Material	Nb <sub>2</sub> O <sub>5</sub>	SiO <sub>2</sub>	Nb <sub>2</sub> O <sub>5</sub>	SiO <sub>2</sub>	Nb <sub>2</sub> O <sub>5</sub>	SiO <sub>2</sub>	Nb <sub>2</sub> O <sub>5</sub>	SiO <sub>2</sub>	Nb <sub>2</sub> O <sub>5</sub>	SiO <sub>2</sub>
Thickness (nm)	23.9	142.3	10.9	45	79	13.7	30.6	152.8	3.2	55.7
Layer #	31	32	33	34						
Material	Nb <sub>2</sub> O <sub>5</sub>	SiO <sub>2</sub>	Nb <sub>2</sub> O <sub>5</sub>	SiO <sub>2</sub>						
Thickness (nm)	40.2	5.7	72.2	104.2						

**Fig. 5** Spectral reflection of visible/near-IR antireflection coating optimized at 45° for the S polarization



- layers 25–34: optical monitoring at 450 nm on test glass 3.

This strategy was then tested by performing simulations using Virtual Deposition Process software as provided by Bühler company [13–15]. Using such a software that includes typical random errors that are obtained with an OMS 5100 optical monitoring system, it is possible to simulate deposition runs and predict the performances of a multilayer structure at achievement. That way, it is possible to test various optical monitoring strategies and choose the one that results, from these simulations, in the best predicted spectral performances. After validation of the optical monitoring strategy, the structure was fabricated using the Bühler HELIOS machine (Run 1). The transmission spectrum was finally measured at normal incidence and 45° angle of incidence for the S and P polarizations (Fig. 6). The wavelength shift between normal and oblique incidence is clearly visible when comparing these two figures. It should be noted that at a 45° angle of incidence, the reflection on the uncoated rear face induces a significant decrease in the transmission of the order of 8% in S polarization while this contribution is negligible in P polarization (0.6%).

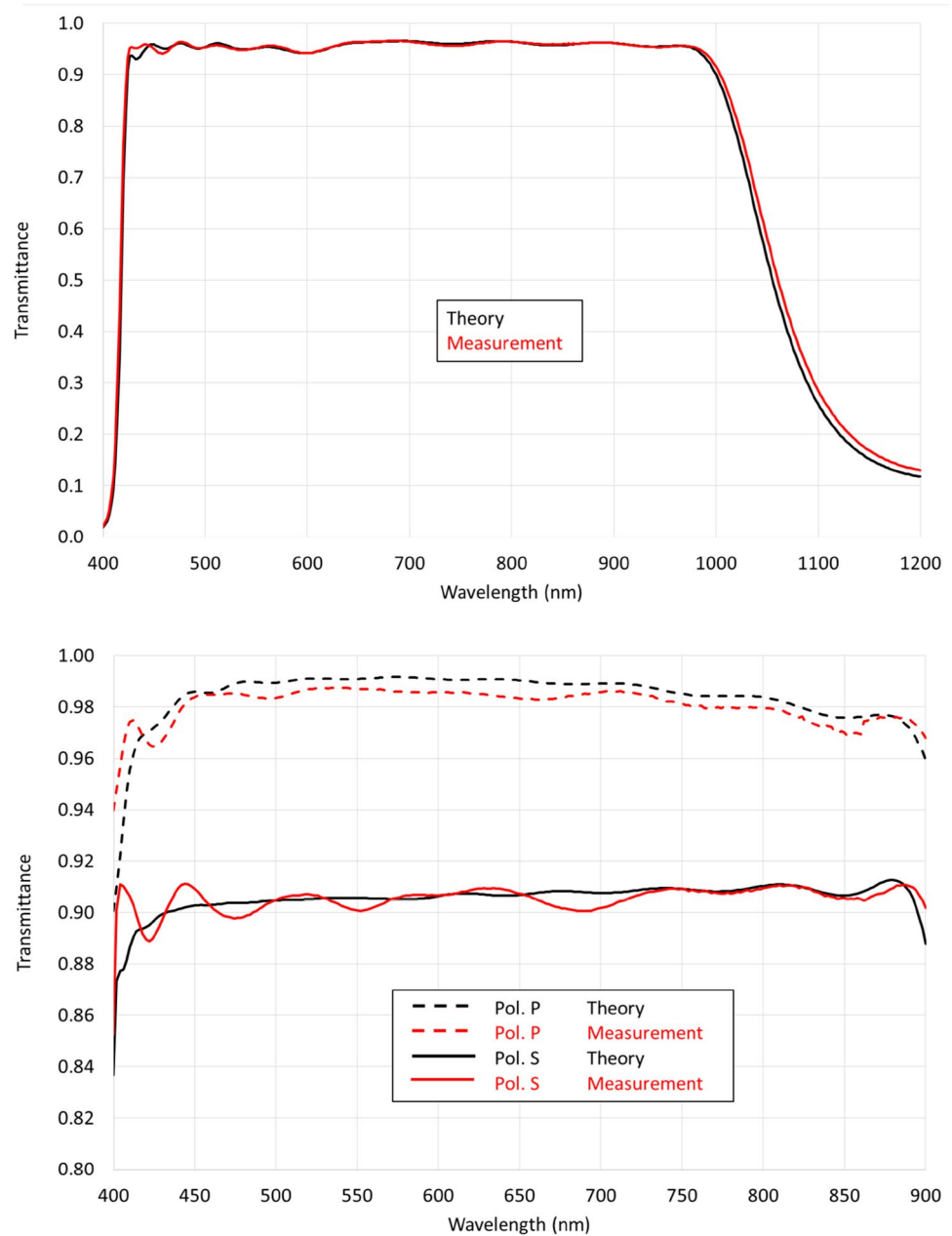
We see that with this optical monitoring method, we have been able to minimize the errors on the layer thicknesses during the deposition of the coating, which guarantees a very good agreement between theoretical and experimental data. Slightly larger discrepancy can be seen at oblique than at normal incidence. We also repeated the manufacturing and monitoring process (Run 2) to fabricate dual-side-coated samples and the spectral response of a dual-side-coated substrate was measured at 45° (Fig. 7, Runs 1 + 2). It can be

seen that with these structures, it is possible to guarantee an average transmission of the order of 97% with fluctuations lower than 1.5% over the spectral range (400–900) nm. Transmission fluctuations are a little larger than those predicted by the theory. This can be explained by the fact that optical monitoring is carried out at normal incidence and errors compensations are made to correct the optical thickness of each layer to achieve optimal performances at normal incidence. Indeed, optical monitoring of non-quarter-wave layers relies on the so-called trigger point monitoring by swing [16, 17], which uses pre-calculated intensity levels to stop the deposition of a given layer. Such a technique uses previously measured optical signal to recalculate the next stopping intensity criterion. In other words, this technique allows producing thickness errors to get better theoretical/experimental agreement at normal incidence. However, at oblique incidence, the effect of thickness errors can generate larger discrepancies in the spectral performances and this would explain the larger, but still quite limited discrepancy between theoretical and experimental curves. This is a classical effect that is generally observed when fabricating polarizing beamsplitters.

### 2.3 Visible/near-IR antireflection coating optimized for beams with large numerical aperture

The last antireflection coating study for the visible/near-IR range concerned the spectral band between 400 and 800 nm considering a beam with aperture up to  $\pm 50^\circ$  (from normal incidence). According to this beam conical geometry, the designs have been optimized simultaneously for different angles of incidence, with a specific weight increasing with

**Fig. 6** Spectral response in the transmission of a visible/near-IR antireflection coating optimized for the S polarization in oblique incidence, deposited on one side, and optically monitored using three test glasses (Run 1). Top figure: measurement at normal incidence. Bottom figure: measurement at 45° incidence



the square of each of these angles. As stated previously, the increase of the angle of incidence produces a spectral shift toward blue and a separation of spectral responses in S and P polarizations. In the case of an open beam that includes many angles of incidence, this means that the spectral range of efficiency must be, for any angle of incidence, larger than specified. The maximum spectral width is, therefore, smaller for an open beam compared with a collimated one. We again considered  $\text{Nb}_2\text{O}_5$  and  $\text{SiO}_2$  as the high- and low-refractive index materials for layers, and fused silica as the substrate. Structures were optimized to minimize the residual reflection for non-polarized light. At first, we studied the evolution of the minimum achievable residual reflection as the

beam aperture is increased. In Table 3, we provide the typical design parameters (total stack thickness and number of layers) and average spectral performances (considering a linear wavelength distribution) of antireflection coatings optimized for non-polarized light. Increasing the beam aperture up to  $40^\circ$  results in a slow and mild increase of the residual reflection by a factor of 2, but this increase reaches a  $4\times$  value if it is further increased up to  $50^\circ$ . Figure 8 gives the spectral dependence of the reflectance of these coatings for non-polarized light. To complete this result, Fig. 9 gives the average residual reflection as a function of the angle of incidence for each polarization. One can clearly see that the S polarization is the major contributor to the reflectance

**Fig. 7** Spectral response in transmission at a  $45^\circ$  angle of incidence of a dual-side visible/near-IR antireflection coating for oblique incidence monitored with three test glasses (Runs 1+2)

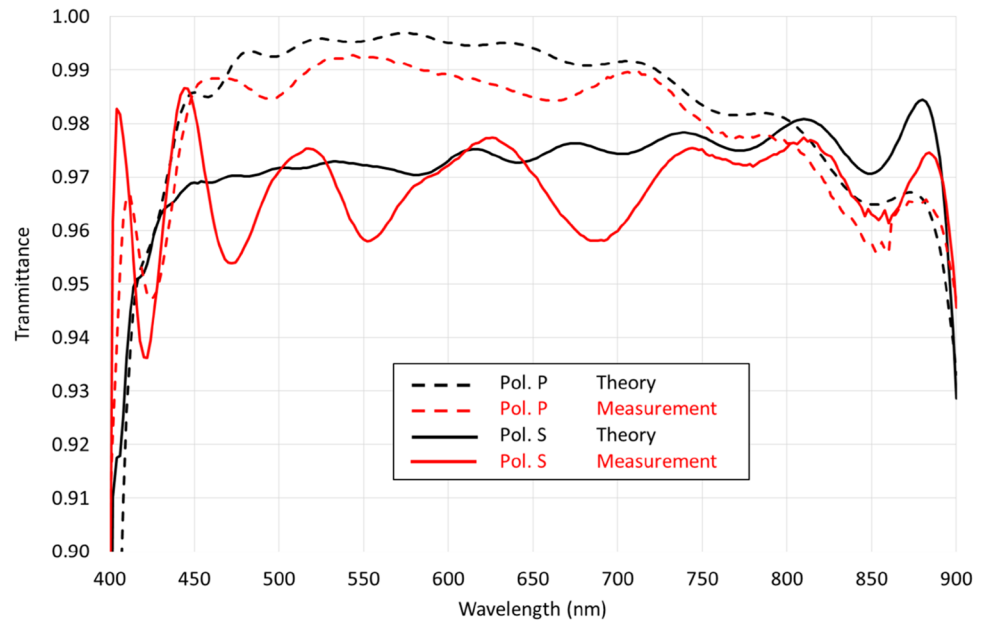


**Table 3** Typical performances of antireflection coatings optimized for oblique incidence

Beam aperture ( $^\circ$ )	Total thickness (nm)	Layer number	Average reflection
$\pm 10$	1684	35	0.0013
$\pm 20$	1616	34	0.0014
$\pm 30$	1543	32	0.0018
$\pm 40$	1622	37	0.0026
$\pm 50$	1730	45	0.0049

increase since the average reflectance for P polarization is rather stable up to  $35^\circ$  angle of incidence. One consequence is that not only the reflectance but also the degree of polarization increases with the angle of incidence. It is worth noting that the design of non-polarizing coatings is a real theoretical difficulty, leading to complex structures with lower performance, involving more than two-layer materials.

Since we are not equipped for optical characterizations in the case of open beam, none of these coatings has been manufactured. However, considering the previous results

**Fig. 8** Spectral reflection of visible/near-IR antireflection coatings for an increasing beam aperture. Each curve is associated with a different optimized design

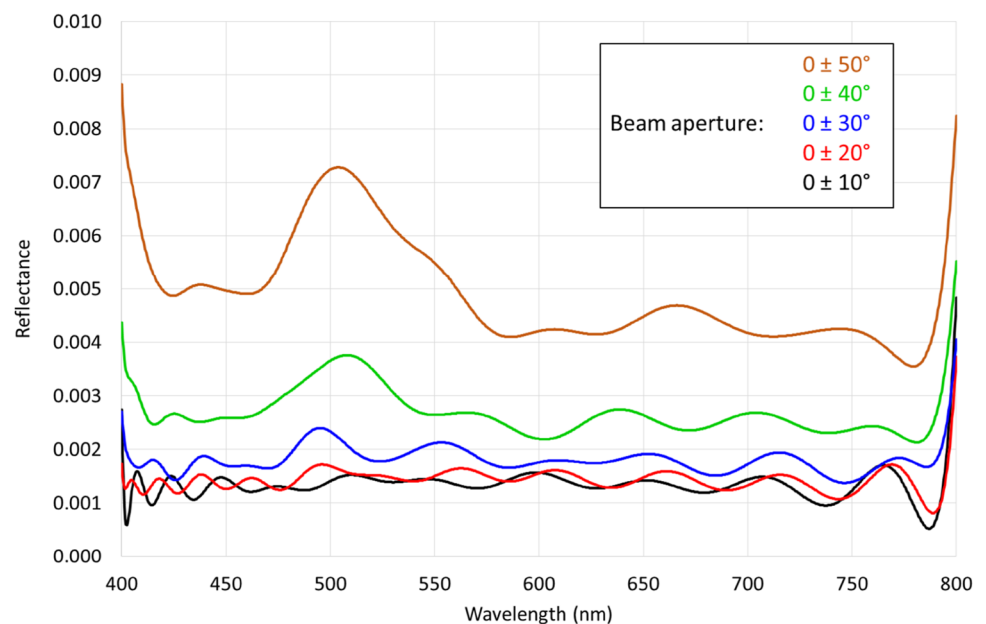
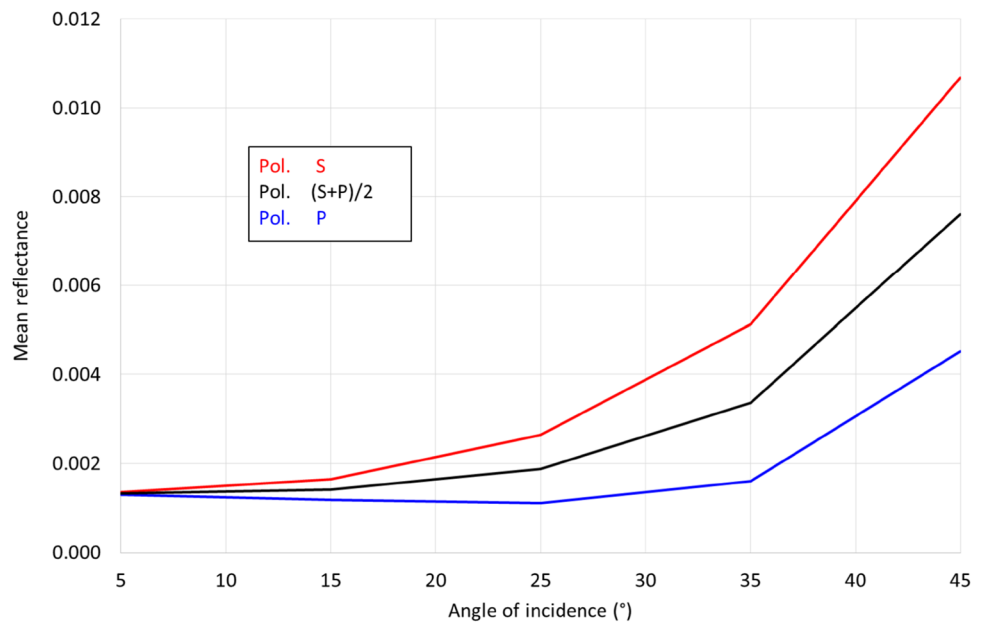




**Fig. 9** Average reflection value of visible/near-IR antireflection coatings for both S and P polarizations. Each angle of incidence is associated with a different optimized design



that have been presented (Sect. 2.2) with similar maximum angle of incidence (45°) and number of layers (34), we are confident in the fact that these calculations are representative of the performances that could be achieved.

### 2.4 Near-IR/mid-IR antireflection coating for normal incidence

The last antireflection coating structure that has been studied was optimized for the spectral band between 1.5 and 15 μm and to minimize the residual reflection at normal incidence of a ZnSe substrate. As illustrated in Fig. 10, the ideal structure for an antireflection coating consists of a gradient of refractive index starting from the substrate index and decreasing to the external medium index. The longer this index transition, the broader the spectral range of such a solution. Following this idea, a multilayer coating is then expected to mimic such a structure, for example with a step index profile. However, using only two materials for layers, this means that each step has to be replaced by a multilayer

structure that behaves similarly and that is formed with these two materials. This can be done classically and efficiently by replacing each step with a three-layer symmetrical stack, provided that the step index value is in between the layer material index values and those layer thicknesses are not too large with respect to the wavelength [14]. From this last condition results the minimum number of step layers that are required to cover the specified spectral range. The final index profile then shows decreasing thicknesses for one material, while thicknesses are increasing for the other, as schematically illustrated in green color in Fig. 10, assuming that external media indices are used also for layers.

In the case of a low-index substrate, such as silica in the previous examples, and using silica as low-index material, there was no possibility to use this gradient index approach. Coatings were, therefore, designed numerically and reflectance was decreased by the mean of destructive interference. The price to pay was a limited spectral range of efficiency.

In the case of a high-index substrate such as ZnSe or Ge ( $n \approx 2.44$  and 4, respectively) that are frequently used in the

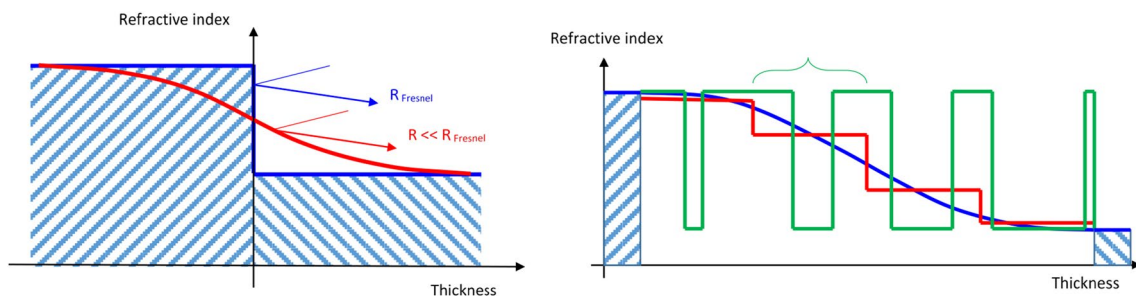


**Fig. 10** Illustration of the AR coating principle for a high-index substrate. Left: schematic representation of a graded index profile. Right: equivalent solution using a step index profile and replacing each step by a “three layer symmetrical high and low index structure”

mid-IR spectral range, and considering that these materials can also be used for high-index layers, it becomes possible to propose a coating that is equivalent to a step index profile, using high-index layers with progressively decreasing thicknesses and conversely low-index layers with progressively increasing thicknesses. Using such a structure, the produced gradient index profile is not really interferential, thus, there is no limitation of the spectral range, provided that the coating is thick enough and formed with layers that are thin enough. However, the equivalent index gradient is limited by layer materials indices, and the mismatch that exists between these material indices and the substrate and external medium indices is responsible for the residual reflectance. Typically, using a 1.5 refractive index value for the low-index material leads to 4% reflectance on the air side, which is similar to an uncoated silicate glass substrate. But the starting reflectance level being much higher, 17% for ZnSe, or even 36% for Ge, the gain is quite important and a lower reflectance level can be expected as the spectral range is reduced.

As an illustration, we have studied an antireflection coating for a ZnSe substrate, using ZnS and YF<sub>3</sub> for layers. The spectral range extends from 1.5 to 15  $\mu\text{m}$ , corresponding to

a 10 $\times$  ratio while the maximum ratio is about 3 $\times$  for a low-index substrate as shown in Sect. 2.1. It is worth noting that contrary to oxide-layer materials, ZnS and YF<sub>3</sub> are not compliant with ion assistance during deposition, which results in a lower packing density, especially concerning YF<sub>3</sub>. One consequence is water adsorption that induces absorption bands at wavelengths 2.9 and 6  $\mu\text{m}$  and also long wavelength absorption beyond 10  $\mu\text{m}$ . Due to absorption, reflectance and transmittance are no more complementary, and the design can be optimized either to minimize reflectance (minimum shadow images in the system) or maximize transmittance (maximum throughput of the system). In such a case, the usual denomination “antireflection coating” might not be adequate according to the coating specification.

The structure given in Table 4 was optimized to give minimum reflectance. It is composed of 14 layers with decreasing ZnS layer thicknesses from 435 to 29.6 nm and increasing YF<sub>3</sub> layer thickness from 30.8 up to 593.5 nm. The stack total thickness is 2.8  $\mu\text{m}$ .

We have plotted in Fig. 11 the theoretical spectral dependence of the transmission and the reflection of the stack in Table 4.

**Table 4** Layer thicknesses of near-IR/mid-IR antireflection coating for normal incidence

Layer #	1	2	3	4	5	6	7
Material	ZnS	YF <sub>3</sub>	ZnS	YF <sub>3</sub>	ZnS	YF <sub>3</sub>	ZnS
Thickness (nm)	435.2	30.8	227.6	74.1	199	121.5	162.4
Layer #	8	9	10	11	12	13	14
Material	YF <sub>3</sub>	ZnS	YF <sub>3</sub>	ZnS	YF <sub>3</sub>	ZnS	YF <sub>3</sub>
Thickness (nm)	176.4	121.6	234.9	77.6	308.3	29.6	593.5

**Fig. 11** Spectral performance of mid-IR antireflection coatings optimized for minimum reflectance (formula provided in Table 4) and maximum transmittance

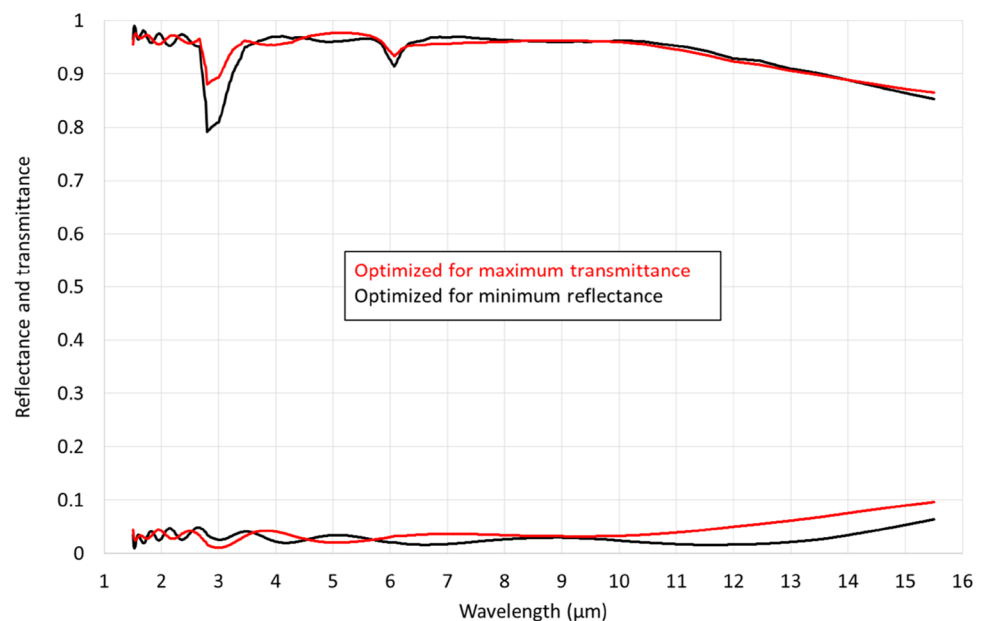


**Table 5** Layer thicknesses of near-IR/mid-IR antireflection coating for normal incidence and optimized in transmission

Layer #	1	2	3	4	5	6	7
Material	ZnS	YF <sub>3</sub>	ZnS	YF <sub>3</sub>	ZnS	YF <sub>3</sub>	ZnS
Thickness (nm)	398.7	15.6	264.5	69.5	173.5	147.7	131.7
Layer #	8	9	10	11			
Material	YF <sub>3</sub>	ZnS	YF <sub>3</sub>	ZnS			
Thickness (nm)	214.8	69.6	440.3	25.6			

The ZnS and YF<sub>3</sub> refractive indices and extinction coefficients used for this calculation can be found in Ref. [3]. The last and thickest YF<sub>3</sub> layer allows to reduce reflectance at the longer wavelength, but induces a significant amount of absorption losses.

The structure given in Table 5 was on the contrary optimized to give maximum transmittance. The layer count is now 11 (minus 3 layers), with a total coating thickness reduced to 1.9  $\mu\text{m}$  (0.9  $\mu\text{m}$  thinner), this thickness reduction mainly concerning YF<sub>3</sub> (0.65  $\mu\text{m}$  thinner).

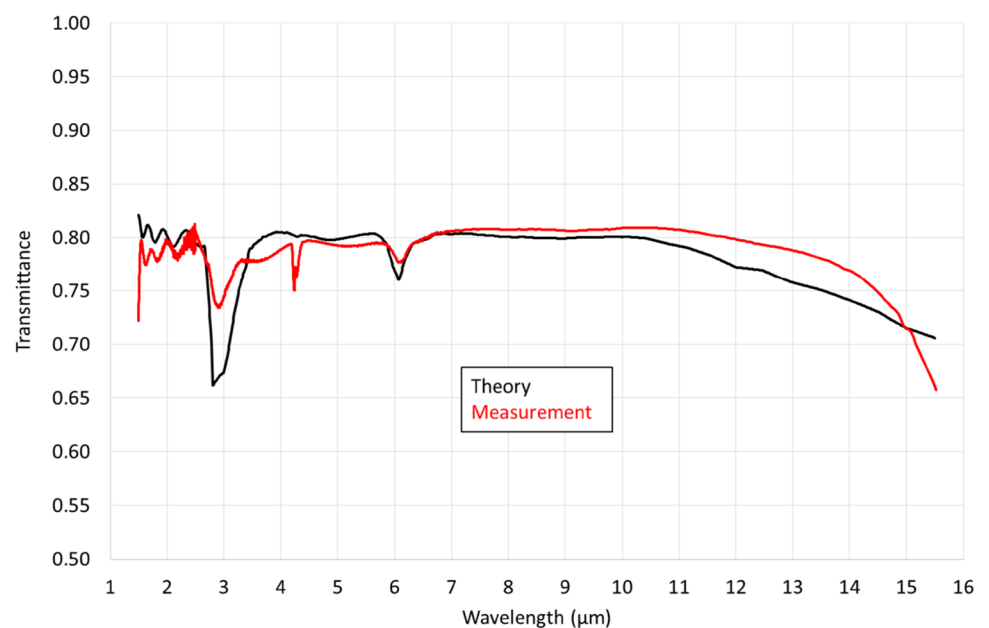
Figure 11 also gives the theoretical reflectance and transmittance curves for this coating. Transmittance is slightly better in absorbing spectral bands at 2.9 and 6  $\mu\text{m}$  and the reflectance increase observed at longer wavelengths (10–15  $\mu\text{m}$ ) is compensated by the reduction of absorption losses so that transmittance is almost unchanged in this spectral region. But the coating has now 11 layers (Table 5) instead of 14, for a total thickness of 1.9  $\mu\text{m}$  instead of 2.8  $\mu\text{m}$ .

One can see that broadband antireflection coating from 1.5 to 15  $\mu\text{m}$  could be achieved. With such a structure, the

average residual reflection on the coated surface is equal to about 3% and up to 5% at 15  $\mu\text{m}$ . Using only a multilayer structure, it is not possible to achieve lower residual reflection coefficient using these materials. Finally, we experimentally demonstrated this class of antireflection coating. The technology chosen to fabricate this structure is non-assisted e-beam deposition. The depositions were carried out using a Bühler SYRUSpro 710 machine within the *Espace Photonique* platform of *Institut Fresnel*. The control of the thickness of each of the layers was carried out using a Bühler OMS 5000 optical monitoring system interfaced with the SYRUSpro machine. Using a dedicated software for the determination of optimal optical monitoring strategy combined with a Virtual Deposition Process software [14–16], the following optical monitoring strategy was determined:

- layers 1–6: optical monitoring at 720 nm;
- layers 7–14: optical monitoring at 740 nm.

**Fig. 12** Spectral response in transmission at normal incidence of a near-IR/mid-IR antireflection coating optimized. For minimum reflectance at normal incidence, deposited on one side of a ZnSe substrate



The transmission spectrum was finally measured at normal incidence using a Fourier transform infrared spectrometer (Fig. 12).

One can see that using this strategy, we have been able to fabricate a broadband antireflection coating covering the whole 1.5–15- $\mu\text{m}$  spectral range. There is a very good agreement between theory and experiment, with absorption losses lower than predicted.

Compared with results presented in Ref. [3] for which the spectral range extended from 3.5 to 16  $\mu\text{m}$  with a seven-layer coating, the spectral width ratio  $\lambda_{\text{max}}/\lambda_{\text{min}}$  is here about twice larger, resulting in a twice more complex structure with 14 layers.

This increase in complexity mainly concerns manufacturing and especially thickness monitoring. Indeed, very thick layers are required to operate at long wavelength (15  $\mu\text{m}$ ), and thickness errors on such thick layers can rapidly represent a significant amount to perturbate optical properties at smaller wavelengths, here ten times smaller (1.5  $\mu\text{m}$ ).

### 3 Conclusion

We have shown the design and the fabrication of broadband antireflection coatings for spectral ranges from visible up to mid-IR ranges. We have demonstrated that using multilayer structures, it is possible to design broadband antireflection structures that can be accurately manufactured using the proper optical monitoring strategy. We have also shown that the materials used for the design and the fabrication of such structures will highly influence the final performances of the antireflection coatings: increasing the spectral region where the antireflection is effective results in an increase of the residual reflection.

**Acknowledgements** This work was carried out within the framework of a Recherche et Technologie (R&T) project funded by the French Space Agency (CNES). This work was partially funded by Centre National d'Etudes Spatiales Grant number R-S13/OT-0006-030.

### References

- Strong, J.: On a method of decreasing the reflection from nonmetallic substances. *J. Opt. Soc. Am.* **26**(1), 73–74 (1936)
- Dobrowolski, J.A., Sullivan, B.T.: Universal antireflection coatings for substrates for the visible spectral region. *Appl. Opt.* **35**, 4993–4997 (1996)
- Lemarquis, F., Marchand, G., Amra, C.: Design and manufacture of low-absorption ZnS–YF<sub>3</sub> antireflection coatings in the 3.5–16- $\mu\text{m}$  spectral range. *Appl. Opt.* **37**, 4239–4244 (1998)
- Dobrowolski, J.A., Guo, Y., Tiwald, T., Ma, P., Poitras, D.: Toward perfect antireflection coatings. 3. Experimental results obtained with the use of Reststrahlen materials. *Appl. Opt.* **45**, 1555–1562 (2006)
- Tan, G., Lee, J.-H., Lan, Y.-H., Wei, M.-K., Peng, L.-H., Cheng, I.-C., Wu, S.-T.: Broadband antireflection film with moth-eye-like structure for flexible display applications. *Optica* **4**, 678–683 (2017)
- Amotchkina, T.V.: Empirical expression for the minimum residual reflectance of normal- and oblique-incidence antireflection coatings. *Appl. Opt.* **47**, 3109–3113 (2008)
- Tikhonravov, A.V., Trubetskov, M.K., DeBell, G.W.: Optical coating design approaches based on the needle optimization technique. *Appl. Opt.* **46**, 704–710 (2007)
- <https://www.fresnel.fr/spip/spip.php?article1159>. Accessed July 2019
- M. Scherer, J. Pistner, Lehnert, W.: UV- and VIS filter coatings by plasma assisted reactive magnetron sputtering (PARMS). In: *Optical Interference Coatings, OSA Technical Digest* (Optical Society of America, 2010), paper MA7
- A. Zoeller, M. Boos, H. Hagedorn, W. Klug, C. Schmitt: High accurate in situ optical thickness monitoring. In: *Optical Interference Coatings, OSA Technical Digest Series* (Optical Society of America, 2004), paper TuE10
- Vignaux, M., Lemarchand, F., Begou, T., Grèzes-Beset, C., Lumeau, J.: Trinary mappings: a new tool for the determination of potential spectral paths for optical monitoring of optical interference filters. *Appl. Opt.* **57**(24), 7012–7020 (2018)
- Vignaux, M., Lemarchand, F., Begou, T., Grèzes-Beset, C., Lumeau, J.: Automated method for the determination of the all-optical monitoring strategy of complex thin-film filters. *Opt. Express* **27**(9), 12373–12390 (2019)
- Berning, P.: Use of equivalent films in the design of infrared multilayer antireflection coatings. *J. Opt. Soc. Am.* **52**, 431–436 (1961)
- Trubetskov, M., Amotchkina, T., Tikhonravov, A.: Automated construction of monochromatic monitoring strategies. *Appl. Opt.* **54**, 1900–1909 (2015)
- Ehlers, H., Ristau, D.: Advanced control and modeling of deposition processes. *Chin. Opt. Lett.* **s1**(11), S10203 (2013)
- A. Zöllner, M. Boos, H. Hagedorn, B. Romanov: Computer simulation of coating processes with monochromatic monitoring. In: *Proceedings of SPIE 7101, Advances in Optical Thin Films III, 71010G* (25 September 2008)
- Macleod, H.A.: *Thin-Film Optical Filters*, 4th edn. Taylor & Francis, Boca Raton (2010)

**Publisher's Note** Springer Nature remains neutral with regard to jurisdictional claims in published maps and institutional affiliations.